Modern Physics Letters A
© World Scientific Publishing Company

IMPLEMENTATION OF THE ATLAS-SUSY-2018-31 ANALYSIS IN THE MADANALYSIS 5 FRAMEWORK

JACK Y. ARAZ

Institute for Particle Physics Phenomenology, Durham University, South Road, Durham, DH1 3LE, UK

jack.araz@durham.ac.uk

BENJAMIN FUKS

Laboratoire de Physique Théorique et Hautes Energies (LPTHE), UMR 7589, Sorbonne Université et CNRS, 4 place Jussieu, 75252 Paris Cedex 05, France

Institut Universitaire de France, 103 boulevard Saint-Michel, 75005 Paris, France

fuks@lpthe.jussieu.fr

We present the implementation, in the MadAnalysis 5 framework, of the ATLAS-SUSY-2018-31 search for new physics, and document the validation of this implementation. This analysis targets, with 139 fb^{-1} of proton-proton collisions at a centre-of-mass energy of 13 TeV recorded by the ATLAS detector between 2015 and 2018, the production of a pair of supersymmetric bottom squarks when they further decay through a cascade decay involving the second lightest neutralino and a Standard Model Higgs boson. The validation of our work is based on three benchmark scenarios targetting different kinematic configuration. The first of them considers a new physics spectrum leading to the presence of high-p_T b-jets originating from sbottom decays, whereas the last two, that differ by the neutralino mass spectrum, are dedicated to the compressed regime and thus yield the presence of soft b-jets in the final state. We obtain an agreement between the MadAnalysis 5 predictions and the official ATLAS results at the level of 20%–30%, the largest discrepancies being related to cases exhibiting a poor Monte Carlo numerical precision at the level of the official ATLAS results.

1. Introduction

The popularity of supersymmetry (SUSY) mostly arises as it provides, by extending the Poincaré algebra and by linking the fermionic and bosonic content the theory, an elegant solution to the hierarchy problem inherent to the Standard Model (SM). In the Minimal Supersymmetric Standard Model (MSSM) [1, 2], each of the SM degree of freedom is associated with a supersymmetric partner. After the breaking of the electroweak symmetry, the partners of the gauge and Higgs fields mix into four neutralino ($\tilde{\chi}^0_{1,2,3,4}$) and two chargino ($\tilde{\chi}^\pm_{1,2}$) mass eigenstates, the lightest neutralino being often taken as a viable candidate for dark matter. In order for the MSSM to consist of a solution for the hierarchy problem, the supersymmetric partners of the top and bottom quarks are in general required to be quite light, so that their

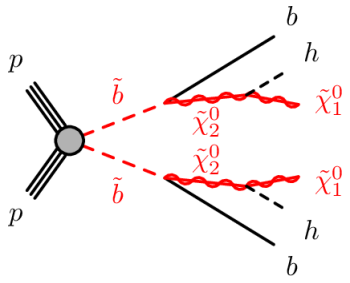

Fig. 1. Representative sbottom pair production, followed by sbottom cascade decays through the second neutralino. The figure has been retrieved from ref. [5].

quadratic contributions to the quantum corrections to the Higgs boson mass stay under control [3,4]. They have thus the possibility to be copiously pair-produced at the LHC.

The ATLAS-SUSY-2018-31 analysis [5] has been designed to investigate the possibility of such light sbottoms, and probes multi-bottom final states additionally featuring a large amount of missing transverse energy. The signature under consideration could arise from sbottom pair production followed by $\tilde{b} \to \tilde{\chi}_2^0 b$ decays, where the second neutralino further decays into an SM Higgs boson and a lightest neutralino,

$$pp \to \tilde{b}\tilde{b}^* \to (\tilde{\chi}_2^0 b)(\tilde{\chi}_2^0 \bar{b}) \to (\tilde{\chi}_1^0 h b)(\tilde{\chi}_1^0 h \bar{b}) \ . \tag{1}$$

A representative Feynman diagram for the above process is shown in figure 1. Such a decay pattern is predicted to be enhanced in MSSM scenarios in which the lightest state $\tilde{\chi}_1^0$ is bino-like and the heavier state $\tilde{\chi}_2^0$ is wino-like, the $\tilde{b} \to \tilde{\chi}_1^0 b$ and $\tilde{b} \to \tilde{\chi}_1^- t$ decays being in this case suppressed. The kinematics of the final-state objects largely depend on the mass spectrum of the various involved particles. Whilst a rather split spectrum gives rise to high-p_T b-jets, a compressed spectrum leads, on the other hand, to relatively soft b-jets.

The ATLAS-SUSY-2018-31 analysis has been divided into three main signal regions SRA, SRB and SRC. Region SRA is dedicated to final states including at least four hard b-jets arising both from Higgs-boson and sbottom decays. Region SRB aims to track relatively softer b-jets which are originating from sbottom decays, together with a harder leading jet dawned from initial-state radiation. Finally, region SRC targets a topology with softer b-jets that are all well separated from the missing energy, which gives rise to a sizeable missing energy significance. This analysis has been found to constrain sbottom masses ranging up to 1.5 TeV in the corresponding simplified models.

In the rest of this note, we present the recast of the ATLAS-SUSY-2018-31 analysis of Ref. [5] in the MadAnalysis 5/SFS framework [6] that relies on smearing and efficiency functions for the simulation of the detector response. The code of our implementation is available from the MadAnalysis 5 dataverse [7], and the Monte

Carlo cards relevant for the validation have been obtained from HEPData [8].

2. Description of the analysis

The considered analysis focuses on a signature made of multiple b-jets and missing transverse energy, which could originate from sbottom pair-production and cascade decays. As mentioned above, the results are interpreted in three classes of simplified models, two of which being relevant for compressed mass spectra and the third one being representative of split spectra. The topology in question is illustrated by figure 1 and by eq. (1).

2.1. *Object definitions*

Jets are obtained by clustering all final-state objects of a given event, with the exception of muons (and invisible particles as the latter are present in typical Monte Carlo event records). Electrons and photons being included, an overlap removal procedure is therefore in order. This is detailed below. Jet clustering relies on the anti-k_T algorithm with a radius parameter set to $R = 0.4$ [9], that is used within the FastJet package version 3.3.3 [10].

Two types of jets are considered in this analysis. First, baseline jets are enforced to have a transverse momentum $p_T > 20$ GeV, and a pseudorapidity satisfying $|\eta| < 4.8$. Signal jets are obtained from this collection, after the object removal procedure described below.

Hadronic taus are extracted from the full jet collection, analysis-level tau candidates having a transverse momentum $p_T > 2.5$ GeV and a pseudorapidity fulfiling $|\eta| < 2.5$. The tau-tagging performance are taken from ref. [11], the tagging efficiency being in average of 60% for a mistagging rate of light jets as hadronic taus of 1%.

The initial sets of leptons are those electrons and muons that are reconstructed from final-state objects after imposing loose electron identification requirements [12], and medium muon identification requirements [13]. Baseline electrons (muons) are then defined from these collections after enforcing that their transverse momentum obeys $p_T > 4.5$ (4) GeV, and their pseudorapidity $|\eta| < 2.47$ (2.5).

In order to clean the jet and lepton collections, first jets are discarded if a baseline electron is found within a distance, in the transverse plane, of $\Delta R \leq 0.2$. Furthermore, baseline electrons and muons are removed if they are found within a distance $\Delta R \leq 0.4$ of a jet.

Signal light jets and b-jets are chosen among the set of cleaned jets. Signal jets are enforced to have a transverse momentum $p_T > 30$ GeV and a pseudorapidity $|\eta| < 2.8$. Any b-tagged jet within this set, with $|\eta| < 2.5$, is considered as an element of the signal b-jet collection. The analysis considers a b-tagging working point involving an efficiency of 77%, for corresponding misidentification rates of 20% for c-jets and 0.9% for lighter-flavour jets [14]. In our simulations, we enforce

the b-tagging algorithm to be based on the presence of a true B-hadron in a cone of radius $\Delta R = 0.3$ around the jet.

Finally, the H_T variable is defined as the scalar sum of the p_T of all jets belonging to the signal jet collection, and the missing momentum vector is defined as the negative vector sum of the p_T of all visible objects.

2.2. *Event selection*

The ATLAS-SUSY-2018-31 analysis includes three main non-orthogonal signal regions denoted SRA, SRB and SRC. Each signal region is dedicated to a specific configuration of the final-state multi-bottom system. Region SRA has been designed to probe quite hard b-jets, typical of a split sbottom-neutralino mass spectrum. Region SRB focuses on softer b-jets as arising from a more compressed mass spectrum, when they are produced in association with a hard initial-state radiation. Finally, region SRC is also dedicated to softer b-jets, but this time when their properties include a large missing energy significance.

All regions include a lepton veto, so that events featuring any baseline electron or muon are rejected. Moreover, one requires that events populating the regions SRA, SRB and SRC respectively feature a number of jets $N_j \geq 6$, 5 and 4. While the selection for regions SRA and SRB asks for the presence of a number of b-jets $N_b \geq 4$, imposes a tau veto and requires a missing transverse energy $\not{E}_T$ greater than 350 GeV, the one for region SRC only asks for at least three b-jets with a missing transverse energy greater than 250 GeV. The preselection finally ends with the requirement that the four leading jets are separated in azimuth from the missing-momentum vector by at least 0.4, in all regions, $\min[\Delta\phi(j_i, \not{E}_T)] > 0.4$ with $i = 1, 2, 3, 4$.

After this preselection, the region SRC is split into several bins of object-based missing transverse energy significance, which we define by $\not{E}_T/\sqrt{H_T}$.

Before being further subdivided into various regions, region SRA selects events featuring a leading b-jet with a p_T of at least 200 GeV, and for which the maximal angular separation between any pair of two b-jets obeys $\Delta R_{max}(b, b) > 2.5$. This defines the pair of b-jets originating from the bottom squark decays. Considering the collection made of all the remaining b-jets, one restricts the minimal angular separation in the transverse plane between any pair made of those b-jets to satisfy $\Delta R_{max-min}(b, b) < 2.5$. This tags the b-jets that are considered to originate from a Higgs-boson decay, the corresponding invariant mass m_h^{reco} being enforced to be larger than 80 GeV. The signal region is finally divided into several bins in the effective mass $m_{\text{eff}} = \not{E}_T + H_T$.

In contrast to the two other sets of regions, region SRB is not further subdivided. It however includes extra cuts. First, the b-jets are organised to form di-jet systems compatible with the decay of the SM Higgs boson. The first Higgs candidate is defined by the pair of b-jets featuring the largest separation ΔR in the transverse plane. Next, the second Higgs candidate is similarly defined from the set of remain-

Table 1. Schematic representation of the cut-flows associated with the three classes of signal regions of the ATLAS-SUSY-2018-31 analysis.

SRA	SRB	SRC
Lepton veto	Lepton veto	Lepton veto
$N_j \geq 6$	$N_j \geq 5$	$N_j \geq 4$
$N_b \geq 4$	$N_b \geq 4$	$N_b \geq 3$
$\not{E}_T > 350$ GeV	$\not{E}_T > 350$ GeV	$\not{E}_T > 250$ GeV
$\min[\Delta\phi(j_{1-4}, \not{E}_T)] > 0.4$	$\min[\Delta\phi(j_{1-4}, \not{E}_T)] > 0.4$	$\min[\Delta\phi(j_{1-4}, \not{E}_T)] > 0.4$
tau veto	tau veto	$\not{E}_T/\sqrt{H_T}$ bins
$p_T(b_1) > 200$ GeV	$\bar{m}_h^{\rm reco} \in [75, 175]$ GeV	
$\Delta R_{max}(b,b) > 2.5$	Leading jet non-b-tagged	
$\Delta R_{max-min}(b,b) < 2.5$	$p_T(j_1) > 350$ GeV	
$m_h^{\rm reco} > 80$ GeV	$\Delta\phi(j_1, \not{E}_T) > 2.8$	
$m_{\rm eff}$ bins	$m_{\rm eff} > 1$ TeV	

ing b-jets. The average invariant mass of those two Higgs candidates $\bar{m}_h^{\rm reco}$ is then imposed to lie in the $[75, 175]$ GeV range. The leading jet is moreover required not to be b-tagged, and to be consistent with a very hard initial-state radiation. Its p_T is hence constrained to be greater than 350 GeV, and this jet has to lie at an azimuthal distance $\Delta\phi(j_1, \not{E}_T) > 2.8$ from the missing momentum vector. Finally, an effective mass of at least 1 TeV is required.

A schematic representation of the definition of all signal regions is shown in table 1.

3. Validation

3.1. *Event generation*

In order to validate our implementation, we consider three scenarios, each of them featuring a spectrum with a different mass splitting and being thus relevant for the validation of a specific class of signal regions. For the signal regions of type SRA, a largely split benchmark point has been used, with masses $m(\tilde{b}, \tilde{\chi}_2^0, \tilde{\chi}_1^0) = (1100, 330, 200)$ GeV. A more compressed spectrum has been choosen for the validation of the implementation of the single signal region SRB, with $m(\tilde{b}, \tilde{\chi}_2^0, \tilde{\chi}_1^0) = (700, 680, 550)$ GeV. Finally, for the class of SRC signal regions, we use a spectrum defined by $m(\tilde{b}, \tilde{\chi}_2^0, \tilde{\chi}_1^0) = (1200, 1150, 60)$ GeV. All SLHA mass spectrum files have been taken from information publicly available from HEPData records that are dedicated to this analysis and that have been provided by the ATLAS collaboration [8].

For our validation, we generate leading-order (LO) event samples for all these

benchmark scenarios with MG5_aMC version 2.7.3 [15], convoluting LO matrix elements with the LO set of NNPDF 2.3 parton distribution functions [16] as driven by the LHAPDF 6 library [17]. Following the Multi-Leg Merging (MLM) prescription [18,19], our samples combine matrix elements describing sbottom pair production in association with up to two extra partons, the merging scale being set to $Q_{\rm match} = m(\tilde{b})/4$. Particle decays, parton showering and hadronisation are dealt by means of Pythia version 8.2 [20], and the simulation of the response of the ATLAS detector has been achieved with the SFS module of MadAnalysis 5 [6]. Our recast can then only be used with MadAnalysis 5 version 1.9.4[a] (or more recent). All analysis files can be obtained from the MadAnalysis 5 dataverse [7]. As in the ATLAS-SUSY-2018-31 publication, we normalise our Monte Carlo samples to cross sections evaluated at the next-to-leading-order in perturbative QCD after matching with threshold resummation at the next-to-leading logarithmic accuracy [21, 22]. The employed cross section values rely on the PDF4LHC15_mc parton distribution functions [23].

3.2. *Comparison with the official results*

In this section, we compare our predictions with the official ATLAS results. Although the different signal regions of the considered analysis overlap, the ATLAS collaboration provides validation material for single regions. This allows us to handle the validation procedure region by region. The quality of our implementation is quantified via the parameter δ defined by

$$\delta_i = \frac{|\varepsilon_i^{\rm ATLAS} - \varepsilon_i^{\rm MA5}|}{\varepsilon_i^{\rm ATLAS}} \ . \tag{2}$$

In this expression, $\varepsilon_i = N_i/N_{i-1}$ represents the relative selection efficiency of the $i^{\rm th}$ cut, with N_i and N_{i-1} being the number of events surviving this cut and the previous one respectively. This parameter is required to satisfy $\delta \lesssim 20\%$ for each cut. Such a level of agreement, that is somewhat arbitrary, is known to only midly impact any limit on a new physics state, due to the steeply falling nature of the cross section with the new physics masses [24]. Moreover, a difference of this order is nevertheless expected from the different detector modeling the simulation chain used in our recast and in the non-public ATLAS software.

Moreover, it is also important to include a measure of uncertainties pertained to the Monte Carlo (MC) event generation process. To quantify this, we define Δ_{MC} as

$$\Delta_{\rm MC} = N_i \sqrt{\frac{1-\epsilon_i}{N_i^{\rm MC}}} \ , \tag{3}$$

[a]The implementation relies on jet energy scale corrections, which have been implemented in MadAnalysis 5 from version 1.9.4.

Table 2. Cut-flow associated with the SRA class of signal regions. The common SRA selection is shown in the first panel of the table, whilst the other panels are dedicated to various $m_{\rm eff}$ bins. For each cut, we present the level of deviation between our predictions and the official ATLAS results δ defined by eq. (2). Moreover, we also report for each $m_{\rm eff}$ bin the corresponding MC uncertainty $\Delta_{\rm MC}$ of eq, (3). We consider a benchmark scenario defined by the mass spectrum $m(\tilde{b}, \tilde{\chi}_2^0, \tilde{\chi}_1^0) = (1100, 330, 200)$ GeV. The ATLAS results correspond to 9,265 MC events prior to any cut, whereas our predictions rely on 165,806 events.

	ATLAS		MadAnalysis 5–SFS		
	Events	ε	Events	ε	δ [%]
Geneator-level	319.7	-	319.7	-	-
Initial	319.7	-	319.7	-	-
Lepton veto	230.5	0.721	216.7	0.678	6.0
$N_j \geq 6$	192.3	0.834	188.9	0.871	4.5
$N_b \geq 4$	87.9	0.457	88.7	0.470	2.7
$\not{E}_T > 350$ GeV	45.1	0.513	49.7	0.560	9.1
$\min[\Delta\phi(j_{1-4}, \not{E}_T)] > 0.4$	20.9	0.463	22.8	0.459	0.9
Tau veto	19.3	0.923	21.7	0.953	3.2
$p_T(b_1) > 200$ GeV	18.2	0.943	20.7	0.950	0.8
$\Delta R_{max}(b,b) > 2.5$	17.6	0.967	20.1	0.975	0.9
$\Delta R_{max-min}(b,b) < 2.5$	15.0	0.852	19.1	0.950	11.5
$m_h^{\rm reco} > 80$ GeV	13.7	0.913	16.1	0.839	8.2
$m_{\rm eff} > 1$ TeV	13.7	1.000	16.1	1.000	0.0
$\Delta_{\rm MC}/N_{\rm yield}$	5.1%		1.2%		
$m_{\rm eff} \in [1, 1.5]$ TeV	0.4	0.029	0.5	0.030	2.4
$\Delta_{\rm MC}/N_{\rm yield}$	28.9%		6.3%		
$m_{\rm eff} \in [1.5, 2]$ TeV	6.4	0.467	5.5	0.344	26.3
$\Delta_{\rm MC}/N_{\rm yield}$	7.8%		1.8%		
$m_{\rm eff} > 2$ TeV	7.0	0.511	10.0	0.626	22.5
$\Delta_{\rm MC}/N_{\rm yield}$	7.1%		1.0%		

where $N_i^{\rm MC}$ is defined as the number of MC events surviving the $i^{\rm th}$ cut, and ϵ_i stands for the cumulative selection efficiency of the $i^{\rm th}$ cut. Here, we emphasise that N_i refers to the number of events surviving the $i^{\rm th}$ cut, after including the signal production cross section and the luminosity under consideration. We aim to constrain $\Delta_{\rm MC} < 10\%$, as this is comparable with the largest MC uncertainty associated with the published ATLAS results.

Our validation results are presented in a twofold way. First, we consider cut-flow tables for all scenarios and the signal region to which they are dedicated. Second,

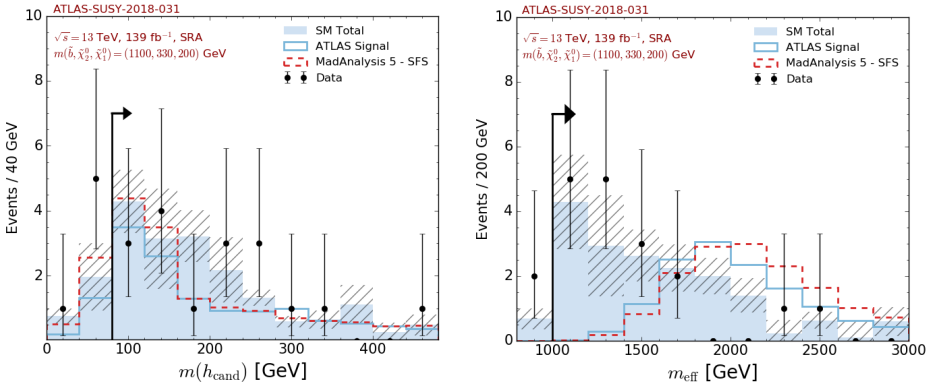

Fig. 2. Histograms representative of the SRA cut-flow. We consider the distribution in the invariant mass of the reconstructed Higgs boson candidate (left) and in the effective mass (right), for a spectrum defined by $m(\tilde{b}, \tilde{\chi}_2^0, \tilde{\chi}_1^0) = (1100, 330, 200)$ GeV. The dashed red line refers to the MadAnalysis 5 predictions, and the blue solid line to the ATLAS official results. As a reference, we show through solid blue bars matched with hatched areas the expected SM background and the related uncertainties, as well as the results emerging from data (black dots).

we present two histograms for each signal region, in which we compare differential distributions that are critical for each region. In our comparison, we use official results and digitised histogram information obtained from HEPData [8]. All cut-flow tables comprise two main columns, one for the ATLAS predictions and one for the MadAnalysis 5 ones. We provide the event counts surviving each cut, together with the relative cut efficiency (ε) and the δ difference between ATLAS and MadAnalysis 5 predictions. We also indicate the MC uncertainties after all requirements (for each bin in the case of the SRA and SRC regions). All tables have been prepared with the `ma5_expert` package [25].

In table 2 and figure 2, we consider the benchmark scenario that is defined by the mass spectrum $m(\tilde{b}, \tilde{\chi}_2^0, \tilde{\chi}_1^0) = (1100, 330, 200)$ GeV and that probes the SRA class of regions. Investigating the cut-flow chart presented in the table, we observe a generally good agreement between our predictions and the official ATLAS results. The largest variations arise in the third and fourth bins in the effective mass m_{eff}, with δ deviations reaching 26% and 23% respectively, for an ATLAS MC uncertainty Δ_{MC} of about 7%–8%. We additionally observe a large MC uncertainty associated with the ATLAS predictions for the second m_{eff} bin, with $\Delta_{\text{MC}} = 29\%$, that is much larger than the difference between the ATLAS and MadAnalysis 5 predictions. This large MC uncertainty is also reflected through shifts in the m_{eff} distributions presented in figure 2 (right panel). In the left panel of the figure, we moreover show the invariant mass of the reconstructed Higgs boson candidate for which the ATLAS and MadAnalysis 5 numbers agree to a good level. In general, we thus observe a good agreement between the ATLAS and MadAnalysis 5 predictions, both at the cut-flow and differential distribution levels, after accounting for the sometimes quite large Monte Carlo uncertainties associated with the public ATLAS results.

Table 3. Same as in table 2 but for the signal region SRB and a spectrum defined by $m(\tilde{b}, \tilde{\chi}_2^0, \tilde{\chi}_1^0) = (700, 680, 550)$ GeV. The ATLAS results correspond to 3,527 MC events prior to any cut, whereas our predictions rely on 149,019 events.

	ATLAS		MadAnalysis 5–SFS		
	Events	ε	Events	ε	δ [%]
Initial	2278.6	-	2278.6	-	-
Lepton veto	1482.6	0.651	1638.4	0.719	10.5
$N_j \geq 5$	943.8	0.637	907.5	0.554	13.0
$N_b \geq 4$	130.2	0.138	145.0	0.160	15.9
$\not{E}_T > 350$ GeV	24.1	0.185	25.1	0.173	6.5
$\min[\Delta\phi(j_{1-4}, \not{E}_T)] > 0.4$	12.8	0.531	12.8	0.510	3.9
Tau veto	12.8	1.000	12.6	0.982	1.8
$\bar{m}_h^{\text{reco}} \in [75, 175]$ GeV	8.5	0.664	7.0	0.559	15.8
Leading jet non-b-tagged	8.5	1.000	5.6	0.802	19.8
$p_T(j_1) > 350$ GeV	7.4	0.871	4.1	0.724	16.9
$\lvert\Delta\phi(j_1, \not{E}_T)\rvert > 2.8$	7.4	1.000	3.2	0.787	21.3
$m_{\text{eff}} > 1$ TeV	7.4	1.000	3.2	0.990	1.0
$\Delta_{\text{MC}}/N_{\text{yield}}$	28.8%		6.9%		

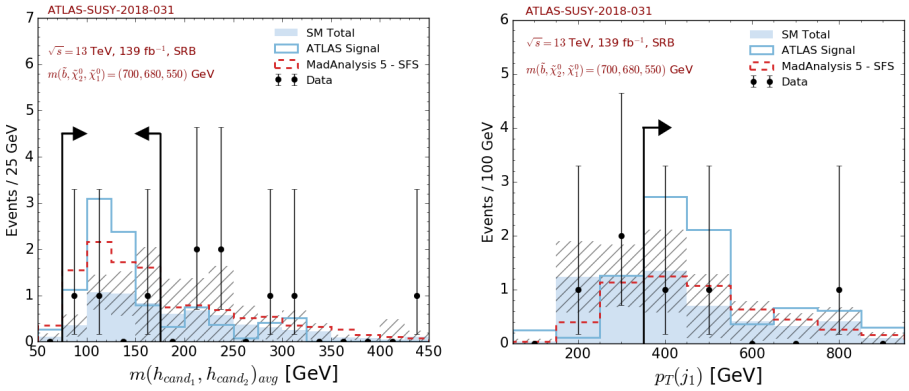

Fig. 3. Histograms representative of the SRB cut-flow. We consider the distribution in the average invariant mass of the Higgs boson candidates (left) and in the p_T of the leading jet (right), for a spectrum defined by $m(\tilde{b}, \tilde{\chi}_2^0, \tilde{\chi}_1^0) = (700, 680, 550)$ GeV. The dashed red line refers to the MadAnalysis 5 predictions, and the blue solid line to the ATLAS official results. As a reference, we show through solid blue bars matched with hatched areas the expected SM background and the related uncertainties, as well as the results emerging from data (black dots).

In table 3 and figure 3, we present results that are relevant for the validation of our implementation of the SRB region, and that have been computed in the

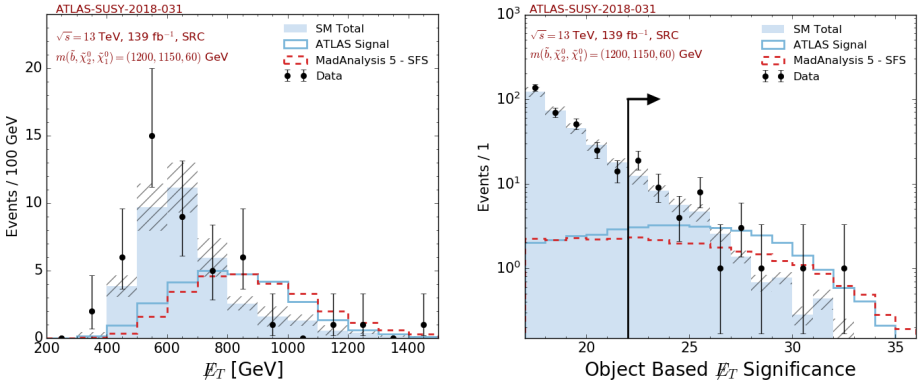

Fig. 4. Histograms representative of the SRC cut-flow. We consider the distribution in the missing transverse energy (left) and in its significance (right), for a spectrum defined by $m(\tilde{b}, \tilde{\chi}_2^0, \tilde{\chi}_1^0) = (1200, 1150, 60)$ GeV. The dashed red line refers to the MadAnalysis 5 predictions, and the blue solid line to the ATLAS official results. As a reference, we show through solid blue bars matched with hatched areas the expected SM background and the related uncertainties, as well as the results emerging from data (black dots).

context of the benchmark scenario defined by the mass spectrum $m(\tilde{b}, \tilde{\chi}_2^0, \tilde{\chi}_1^0) = (700, 680, 550)$ GeV. In terms of the various cut efficiencies shown in table 3, we observe deviations δ between our MadAnalysis 5 predictions and the ATLAS official results that reach up to 21%. However, the ATLAS reference numbers are coming with a quite large MC uncertainty $\Delta_{\rm MC}$ of 28%. The situation is further emphasised in figure 3, in which we present in particular the transverse momentum distribution of the leading jet (right panel). The MadAnalysis 5 (red dashed lines) and ATLAS predictions indeed quite differ in the low p_T regime that is relevant for the cut-flow. Focusing on the second distribution shown in the figure, one may be tempted to naively conclude that the shape of the $\bar{m}_h^{\rm reco}$ observable is on the contrary pretty well reproduced (left panel). The ATLAS curve however features fluctutations and quite differs from the MadAnalysis 5 results in the region that is relevant for the cut-flow. After accounting for the uncertainties on the ATLAS numbers, we cannot therefore draw any strong conclusion about the validation of our implementation. As the related MadAnalysis 5 code is similar to that relevant for the SRA and SRC regions for which good agreement is found (see above and below), we nevertheless consider our implementation as validated. The lack of publc information prevents us from investigating this problem more deeply.

In table 4 and figure 4, we finally turn to the validation of the implementation of the last class of signal regions, the SRC regions, for which we consider a benchmark scenario featuring $m(\tilde{b}, \tilde{\chi}_2^0, \tilde{\chi}_1^0) = (1200, 1150, 60)$ GeV. Both our predictions and the official ATLAS numbers are here numerically accurate, $\Delta_{\rm MC}$ being small. Our predictions are found to agree quite well with the ATLAS predictions, both for the cut-flow tables, the $\not{E}_T$ spectrum and the missing transverse energy significance

Table 4. Same as in table 2 but for the signal region SRC and a spectrum defined by $m(\tilde{b}, \tilde{\chi}_2^0, \tilde{\chi}_1^0) = (1200, 1150, 60)$ GeV. The ATLAS results correspond to 9,668 MC events prior to any cut, whereas our predictions rely on 64,305 events.

	ATLAS		MadAnalysis 5–SFS		
	Events	ε	Events	ε	δ [%]
Initial	180.3	-	180.3	-	-
Lepton veto	127.5	0.707	129.6	0.719	1.7
$N_j \geq 4$	117.1	0.918	120.8	0.932	1.5
$N_b \geq 3$	67.9	0.580	61.9	0.513	11.6
$\not{E}_T > 250$ GeV	61.5	0.906	56.3	0.910	0.5
$\min[\Delta\phi(j_{1-4}, \not{E}_T)] > 0.4$	50.4	0.820	45.6	0.810	1.2
$\not{E}_T/\sqrt{H_T} > 22\ \sqrt{\text{GeV}}$	26.7	0.530	26.3	0.577	9.0
$\Delta_{\text{MC}}/N_{\text{yield}}$	2.2%		1.1%		
$\not{E}_T/\sqrt{H_T} \in [22, 24]\ \sqrt{\text{GeV}}$	6.7	0.133	5.8	0.126	4.8
$\Delta_{\text{MC}}/N_{\text{yield}}$	4.5%		1.7%		
$\not{E}_T/\sqrt{H_T} \in [24, 26]\ \sqrt{\text{GeV}}$	6.4	0.127	5.8	0.126	0.7
$\Delta_{\text{MC}}/N_{\text{yield}}$	4.7%		1.7%		
$\not{E}_T/\sqrt{H_T} >\in [26, 28]\ \sqrt{\text{GeV}}$	5.5	0.109	5.1	0.112	2.9
$\Delta_{\text{MC}}/N_{\text{yield}}$	5.5%		1.9%		
$\not{E}_T/\sqrt{H_T} > 28\ \sqrt{\text{GeV}}$	8.2	0.163	8.1	0.178	9.2
$\Delta_{\text{MC}}/N_{\text{yield}}$	4.9%		1.2%		

spectrum.

4. Conclusions

In this note, we presented our efforts on the implementation of the ATLAS-SUSY-2018-31 analysis in the MadAnalysis 5 framework, using the SFS detector simulation based on smearing and efficiency functions that is shipped with MadAnalysis 5. We have validated our work in the context of three simplified models dedicated to the production and decay of supersymmetric partners of the bottom quark. The validation has been achieved by comparing predictions obtained with our implementation to official results from the ATLAS collaboration. A reasonable agreement has been achieved for each signal region, the deviations remaining in general under a level of 20%–30%. The most considerable discrepancies can be traced to MC uncertainties inherent to the official ATLAS results, hindering hence our capacity to properly validate the implementation of one of the analysis signal regions. The good agreement obtained for all other regions, relying on the same piece of code, nevertheless makes us considering this analysis as validated.

The MadAnalysis 5 C++ code is available from the MadAnalysis 5 dataverse (https://doi.org/10.14428/DVN/IHALED) [7]. The material relevant for the validation benchmarks has been obtained from HEPData [8].

Acknowledgments

The authors are grateful to Laura Jeanty and Federico Meloni for their help with understanding the ATLAS analysis considered in this work. JYA has received funding from the European Union's Horizon 2020 research and innovation programme as part of the Marie Sklodowska-Curie Innovative Training Network MCnetITN3 (grant agreement no. 722104).

References

1. H. P. Nilles, *Phys. Rept.* **110**, 1 (1984).
2. H. E. Haber and G. L. Kane, *Phys. Rept.* **117**, 75 (1985).
3. E. Witten, *Nucl. Phys. B* **188**, 513 (1981).
4. R. Barbieri and G. Giudice, *Nucl. Phys. B* **306**, 63 (1988).
5. ATLAS Collaboration, G. Aad *et al.*, *JHEP* **12**, 060 (2019), arXiv:1908.03122 [hep-ex].
6. J. Y. Araz, B. Fuks and G. Polykratis (6 2020), arXiv:2006.09387 [hep-ph].
7. B. Fuks and J. Y. Araz, *10.14428/DVN/IHALED* (2020).
8. ATLAS Collaboration, *10.17182/hepdata.89408.v2* (2019).
9. M. Cacciari, G. P. Salam and G. Soyez, *JHEP* **04**, 063 (2008), arXiv:0802.1189 [hep-ph].
10. M. Cacciari, G. P. Salam and G. Soyez, *Eur. Phys. J. C* **72**, 1896 (2012), arXiv:1111.6097 [hep-ph].
11. ATLAS Collaboration, *ATLAS-CONF-2017-029* (5 2017).
12. ATLAS Collaboration, G. Aad *et al.*, *JINST* **14**, P12006 (2019), arXiv:1908.00005 [hep-ex].
13. ATLAS Collaboration, G. Aad *et al.*, *Eur. Phys. J. C* **76**, 292 (2016), arXiv:1603.05598 [hep-ex].
14. ATLAS Collaboration, G. Aad *et al.*, *Eur. Phys. J. C* **79**, 970 (2019), arXiv:1907.05120 [hep-ex].
15. J. Alwall, C. Duhr, B. Fuks, O. Mattelaer, D. G. Öztürk and C.-H. Shen, *Comput. Phys. Commun.* **197**, 312 (2015), arXiv:1402.1178 [hep-ph].
16. NNPDF Collaboration, R. D. Ball, V. Bertone, S. Carrazza, L. Del Debbio, S. Forte, A. Guffanti, N. P. Hartland and J. Rojo, *Nucl. Phys. B* **877**, 290 (2013), arXiv:1308.0598 [hep-ph].
17. A. Buckley, J. Ferrando, S. Lloyd, K. Nordström, B. Page, M. Rüfenacht, M. Schönherr and G. Watt, *Eur. Phys. J. C* **75**, 132 (2015), arXiv:1412.7420 [hep-ph].
18. M. L. Mangano, M. Moretti, F. Piccinini and M. Treccani, *JHEP* **01**, 013 (2007), arXiv:hep-ph/0611129.
19. J. Alwall, S. de Visscher and F. Maltoni, *JHEP* **02**, 017 (2009), arXiv:0810.5350 [hep-ph].
20. T. Sjöstrand, S. Ask, J. R. Christiansen, R. Corke, N. Desai, P. Ilten, S. Mrenna, S. Prestel, C. O. Rasmussen and P. Z. Skands, *Comput. Phys. Commun.* **191**, 159 (2015), arXiv:1410.3012 [hep-ph].

21. B. Fuks, M. Klasen, D. R. Lamprea and M. Rothering, *JHEP* **10**, 081 (2012), arXiv:1207.2159 [hep-ph].
22. B. Fuks, M. Klasen, D. R. Lamprea and M. Rothering, *Eur. Phys. J. C* **73**, 2480 (2013), arXiv:1304.0790 [hep-ph].
23. J. Butterworth *et al.*, *J. Phys. G* **43**, 023001 (2016), arXiv:1510.03865 [hep-ph].
24. B. Dumont, B. Fuks, S. Kraml, S. Bein, G. Chalons, E. Conte, S. Kulkarni, D. Sengupta and C. Wymant, *Eur. Phys. J. C* **75**, 56 (2015), arXiv:1407.3278 [hep-ph].
25. J. Y. Araz, *https://github.com/jackaraz/ma5_expert* (2020).